# Study on printing quality improvement for continuous-type inkjet printer using multi-objective genetic algorithm and ink droplet trajectory simulation

*Koma Sato[1], Eiji Ishii[1], Nobuhiro Harada[2] and Tsuneaki Takagishi[2]*

*[1]Center for Technology Innovation-Mechanical Engineering, Hitachi Ltd., Hitachinaka, Ibaraki, Japan*
*[2]Marking Systems and Hoist Systems Division, Hitachi Industrial Equipment Systems Co., Ltd., Hitachi, Ibaraki, Japan*

## Abstract

*Continuous-type inkjet printers (CIJPs) can be used to print on surfaces with various shapes at high speeds without contacting the printing target. Recently, the need for CIJPs with higher speeds and quality to speed up industrial production lines has been increasing. By increasing the exciting frequency of the piezo element, the ink droplet generation cycle can be shorter, thereby increasing the printing speed. However, as the distance between each charged ink droplet becomes shorter, forces such as air drag and Coulomb repulsion can greatly affect the trajectories of the droplets and may deteriorate the printing quality. To determine the optimal particle injection pattern, we developed an automatic design technique with a multi-objective genetic algorithm (MOGA) and ink droplet trajectory simulation and applied it to the character "7" in a 5 × 5 dot matrix. A MOGA with 20 populations and four generations was performed, and it was confirmed that the developed technique could automatically improve the printing quality of the character. Additionally, correlation analysis was applied to the data obtained from the optimization and some printing control rules to improve the quality were extracted. By applying the rules to the character "3" and "5," it was revealed that the printing qualities of those characters could be also improved.*

## Introduction

Continuous-type inkjet printers (CIJPs) can be used to print on surfaces with various shapes at high speeds without contacting the printing target. In addition, it can be applied to several materials such as metal, paper, glasses, etc., by selecting an appropriate ink. Therefore, CIJPs are widely used to print barcodes and production dates on industrial production lines.

Recently, the need for CIJPs with higher speeds and quality to help speed up industrial production lines has been increasing. By increasing the exciting frequency of the piezo element, the ink droplet generation cycle can be shorter, thereby increasing the printing speed. However, as the distance between each charged ink droplet becomes shorter, forces such as air drag and Coulomb repulsion can greatly affect the trajectories of the droplets and may deteriorate the printing quality.

The authors have developed a technique for predicting the trajectories of the ink droplets using a multi-physics simulation, which considers particle-fluid-electric interaction, and investigated how printing quality could be improved [1]. To improve the printing quality, adjustments are needed to reduce air drag and Coulomb repulsion, which affect the trajectories of the ink droplets. However, these forces are non-linear, so the adjustments are complex. In this study, in order to automatically determine the correct adjustment procedure, we developed a design technique for the ink droplet injection pattern using a multi-objective genetic algorithm (MOGA [4]) and the ink droplet trajectory simulation method mentioned above that focuses on the distance between the charged ink droplets.

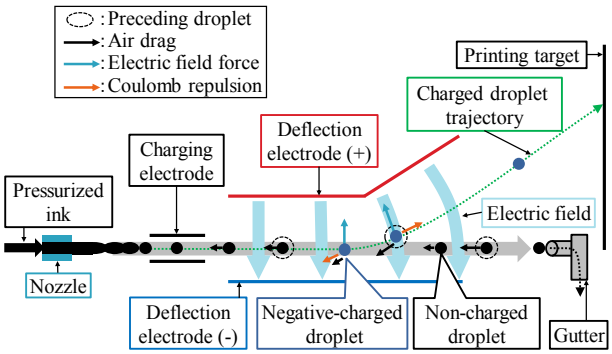


***Figure 1.*** *Printing principle of CIJPs and the external forces on ink droplets.*

## Optimization procedure

In this study, the printing quality of a target character, "7," expressed in a 5 × 5 dot matrix was optimized. The injection order of the charged ink droplets, which composes the character, was fixed, and the number and injection timings of the non-charged ink droplets between the charged ink droplets were the optimization targets.

The sum of the height error of each droplet and that of the distance error of the adjacent ink droplets on the target were objective functions. These two errors were calculated from ideal hit positions on the printing target of each droplet and evaluated by the ink droplet trajectory simulation. A MOGA was performed to minimize these errors, improve the printing quality, and find the optimal ink droplet injection pattern which is the injection order of the charged and non-charged droplets.

Correlation analysis was then applied to the data obtained in the optimization process, and the rules for improving printing quality were extracted. These rules were applied to other characters such as "3" and "5," and the ink droplet trajectory simulations were performed. The details of these procedures are explained below.

### *Simulation method*

To evaluate the hit positions of the charged droplets of a printing target, an ink droplet trajectory simulation developed by the authors was performed [1]. In this simulation, droplets were modeled as Lagrangian particles and a three-dimensional fluid simulation with incompressible and isothermal conditions was performed. Unsteady flow was calculated by using the pressure implicit with splitting of operator (PISO) method [5]. The

incompressible Navier-Stokes equation of fluid for laminar flow is

$$\frac{\partial \alpha \boldsymbol{u}_f}{\partial t} + \nabla \cdot (\alpha \boldsymbol{u}_f \boldsymbol{u}_f) - \nabla \cdot \alpha \boldsymbol{\tau} = -\nabla \frac{p}{\rho_f} - \frac{\boldsymbol{F}}{\rho_f}, \quad (1)$$

where $\alpha$ is gas volume fraction, $t$ is time, $\boldsymbol{u}_f$ is fluid velocity, $\boldsymbol{\tau}$ is stress tensor, $p$ is fluid pressure, $\rho_f$ is fluid density, and $\boldsymbol{F}$ is external forces on ink droplets. Additionally, the following continuity equation must be satisfied

$$\frac{\partial \alpha}{\partial t} + \nabla \cdot (\alpha \boldsymbol{u}_f) = 0. \quad (2)$$

The momentum exchange between the fluid and droplets are done via $\boldsymbol{F}$ in Eq. (1). $\boldsymbol{F}$ is the sum of the three external forces on droplets.

1. Air drag $\boldsymbol{F}_{dr}$

Assuming the droplets are spherical, the equation for air drag can be written as follows:

$$\boldsymbol{F}_{dr} = \frac{3}{4} m_s C_d Re_s \frac{\mu_f}{\rho_s d_s^2} |\boldsymbol{u}_f - \boldsymbol{u}_s|, \quad (3)$$

where $m_s$ is the mass of a droplet, $C_d$ is air drag coefficient, $Re_s$ is the particle Reynolds number, $\mu_f$ is fluid viscosity, $\rho_s$ is droplet density, $d_s$ is droplet diameter, and $\boldsymbol{u}_s$ is droplet velocity. The particle Reynolds number is calculated as $Re_s = |\boldsymbol{u}_f - \boldsymbol{u}_s|/\nu_f$, where $\nu_f$ is fluid kinematic viscosity.

Since the $Re_s$ of ink droplets were less than approximately 200, we introduced Beard's $C_d$ empirical equation, which is accurate within the range of $Re_s < 1000$.

$$C_d = \begin{cases} (24/Re_s)(1 + 0.102 Re_s^{0.955}) & (0.2 < Re_s \le 2.0) \\ (24/Re_s)(1 + 0.115 Re_s^{0.802}) & (2.0 < Re_s \le 21) \\ (24/Re_s)(1 + 0.189 Re_s^{0.632}) & (21 < Re_s \le 200) \end{cases}. \quad (4)$$

Moreover, in accordance with the positions and flight directions of the droplets, the $C_d$ calculated by Beard's equation was modified. Specifically, when two droplets are sufficiently near and flying in roughly the same direction, the $C_d$ of the following droplet decreases since it was influenced by the wake of the preceding droplet, thus, the $C_d$ of the following droplet must be modified. In this study, a $C_d$ modification curve was introduced, which was fitted to Tsuji's experimental results [3]. Figure 2 shows the relation between the non-dimensional distance and the modified coefficient for the $C_d$ calculated by Eq. (4). The non-dimensional distance $L/d_s$ is the distance between the preceding droplet and the following droplet divided by the droplets' diameter. Whether the following droplet is influenced by the wake of the preceding droplet was determined by the position and velocity vector of the preceding droplet and the position of the following droplet, as shown in Fig. 3. When $L/d_s < 10$ and the angle between the difference of the position vectors of the two droplets and the velocity vector of the preceding droplet $\theta_w$ was within 175–180 degrees, the $C_d$ of the following droplet was modified using the curve shown in Fig. 2.

2. Coulomb repulsion $\boldsymbol{F}_{cl}$

Coulomb repulsion can be calculated as follows:

$$\boldsymbol{F}_{cl} = \sum_i \frac{1}{4\pi\epsilon_0} \frac{q q_i}{|\boldsymbol{x} - \boldsymbol{x}_i|^3} (\boldsymbol{x} - \boldsymbol{x}_i), \quad (5)$$

where $i$ is the droplet identifier, $\epsilon_0$ is the permittivity of vacuum, $q$ is the charge of the focused droplet, $q_i$ is the charge of the $i$-th droplet, $\boldsymbol{x}$ is the position vector of the focused droplet, and $\boldsymbol{x}_i$ is the position vector of the $i$-th droplet.

3. Electric force $\boldsymbol{F}_{el}$

Electric force can be calculated as follows:

$$\boldsymbol{F}_{el} = q\boldsymbol{E}, \quad (6)$$

where $\boldsymbol{E}$ is static electric field.

The three forces are summed and substituted into Eq. (1).

$$\boldsymbol{F} = \boldsymbol{F}_{dr} + \boldsymbol{F}_{cl} + \boldsymbol{F}_{el}. \quad (7)$$

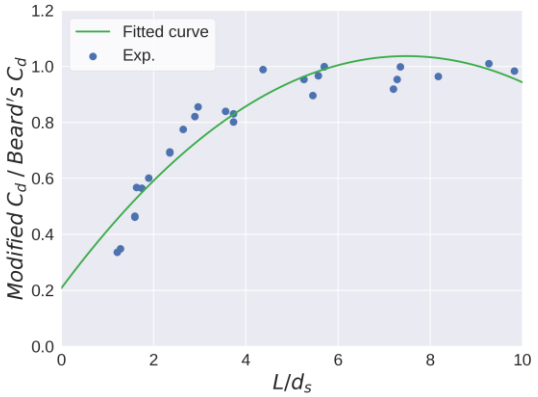


***Figure 2.*** *Drag coefficient modifying curve for a following droplet.*

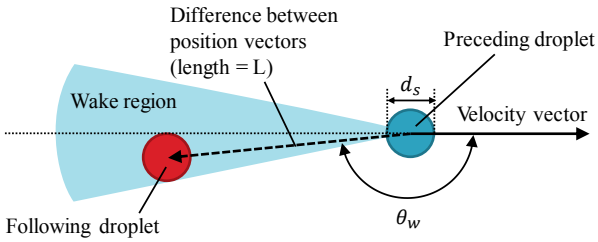


***Figure 3.*** *Values to determine whether the $C_d$ of the following droplet is to be modified.*

## *Optimization method*

To improve the printing quality automatically, a real-coded multi-objective genetic algorithm (MOGA) was performed in the ink droplet trajectory simulation. The design variables controlled the number of non-charged droplets between the charged droplets. The objective functions were the sum of the height errors and the sum of the errors from the ideal distance between droplets on the printing target.

1. Design variables

Figure 4 shows the character "7" in a 5 × 5 dot matrix. Hereafter, the dot in $i$-th column and $j$-th row is dot $ij$.

The injection order of the charged droplets was fixed in the order of 15, 25, 35, 32, 31, 45, 43, 55, and 54 as shown in Fig. 4. Moreover, two additional non-charged droplets were assigned to each column, bringing the number of total droplets of each column to 7. Design variables were defined to arbitrarily control the number of the non-charged droplets to the sequential charged droplets. The candidates representing the non-charged droplet injection timing were 14 positions shown as ① – ⑭ in Fig. 5.

The numbers of the non-charged droplet at each injection timing position were defined by the formulas shown in Table 1. The design variables of the MOGA, $\alpha_i$ $(0 \le \alpha_i \le 1, i = 1, \cdots, 9)$, define the remaining non-charged droplets used in each column. "*round*" denotes the function that rounds the real value off to the nearest whole number. To fix the total number of charged non-charged droplets to 7, the number of non-charged droplets at the last injection timing position in each column was inductively determined depending on the number of droplets already injected. Defining the design variables as described above, all injection patterns can be expressed under two conditions; the injection order of the charged droplets is fixed, and the total number of the droplets for each column is fixed to 7. The baseline injection pattern as a comparison standard is shown in Fig. 6. The baseline is a pattern that injects two non-charged droplets at the beginning of each column and injects the charged and non-charged droplets following the dot matrix pattern shown in Fig. 4; the non-charged droplets were injected at the timing positions of the white space in the dot matrix.

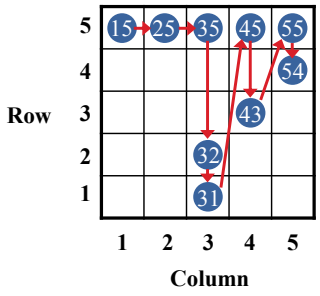


***Figure 4.*** *Character "7" in a 5 × 5 dot matrix. Arrows show injection order of charged droplets.*

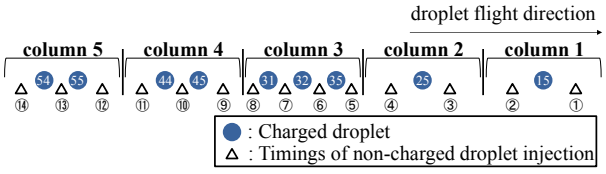


***Figure 5.*** *Candidates of non-charged droplet injection timing. The design variables $\alpha_1, \cdots, \alpha_9$ control the number of non-charged droplets at each timing position.*

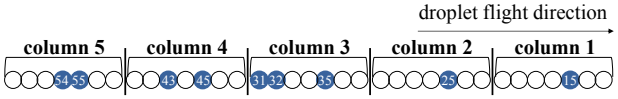


***Figure 6.*** *Baseline injection pattern. White circles are non-charged droplets.*

**Table 1:** Number of non-charged droplets

| Timing | Non-charged droplets | |
|---|---|---|
| | Number | Formula |
| ① | $N_1$ | $round(7 - N_{tgt1}) \times \alpha_1$ |
| ② | $N_2$ | $7 - N_{tgt1} - N_1$ |
| ③ | $N_3$ | $round(7 - N_{tgt2}) \times \alpha_2$ |
| ④ | $N_4$ | $7 - N_{tgt2} - N_2$ |
| ⑤ | $N_5$ | $round(7 - N_{tgt3}) \times \alpha_3$ |
| ⑥ | $N_6$ | $round(7 - N_{tgt3} - N_5) \times \alpha_4$ |
| ⑦ | $N_7$ | $round(7 - N_{tgt3} - N_5 - N_6) \times \alpha_5$ |
| ⑧ | $N_8$ | $7 - N_{tgt3} - N_5 - N_6 - N_7$ |
| ⑨ | $N_9$ | $round(7 - N_{tgt4}) \times \alpha_6$ |
| ⑩ | $N_{10}$ | $round(7 - N_{tgt4} - N_9) \times \alpha_7$ |
| ⑪ | $N_{11}$ | $7 - N_{tgt4} - N_9 - N_{10}$ |
| ⑫ | $N_{12}$ | $round(7 - N_{tgt5}) \times \alpha_8$ |
| ⑬ | $N_{13}$ | $round(7 - N_{tgt5} - N_{12}) \times \alpha_9$ |
| ⑭ | $N_{14}$ | $7 - N_{tgt5} - N_{12} - N_{13}$ |

2. Objective functions

As indicators of the printing quality, the two objective functions were evaluated from the hit positions on a printing target obtained from the ink droplet trajectory simulation.

(a) Height error sum

For every charged droplet on a printing target shown in Fig. 7(a), the ideal hit heights were defined. Height errors were calculated as the distance between the ideal hit heights and the hit heights obtained from the ink droplet trajectory simulation. $h_j$ $(j = 1, \cdots 5)$ denotes the ideal hit height corresponding to the dot in the $j$-th row. The errors of each charged droplet were summed and minimized by the MOGA.

(b) Adjacent distance error sum

The ideal distances between sequential charged droplets, such as between dots 15 and 25, 25 and 35, 35 and 32, and so on, were specified beforehand. The error was then calculated as the distance between the ideal distance and the distance obtained from the ink droplet trajectory simulation as shown in Fig. 7(b). $d_k$ $(k = 1, \cdots 8)$ is the ideal distance between each combination of sequential charged droplets. For example, the error between dots 15 and 25 is calculated with $|d_1' - d_1|$. $d_1$, $d_2$, $d_4$, $d_7$ are the ideal horizontal distances and $d_3$, $d_5$, $d_6$, $d_8$ are the ideal longitudinal distances.

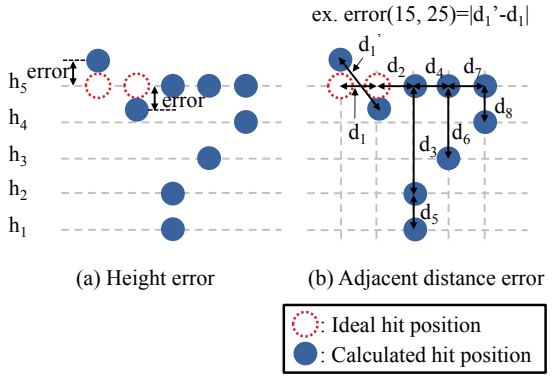


***Figure 7.*** *Definitions of objective functions. Two summed errors from ideal hit positions and ideal distances were evaluated from the results obtained from the ink droplet trajectory simulation.*

3. Optimization procedure

Figure 8 shows the flow of the optimization. The details of each procedure are described below. The MOGA setting is shown in Table 2.

(a) Create initial generation

The design variable set of the MOGA initial generation was created. As a design variable, $\alpha_i$ $(0 \leq \alpha_i \leq 1, i = 1, \cdots, 9)$ is introduced and the initial generation is created by Latin hypercube sampling [6].

(b) Determine ink droplet injection pattern

From the initial generation, the numbers of non-charged droplet at each injection timing position shown in Fig. 5 are determined.

(c) Execute ink droplet trajectory simulation

On the basis of the ink droplet injection pattern, the ink droplet trajectory simulation is executed.

(d) Evaluate objective functions

The two objective functions described in Fig. 7 are calculated from the hit positions on the printing target of the simulation results.

(e) Determine finishing condition

The optimization continues until the MOGA generation reaches the specified number.

(f) Create next generation

The next generation is created by the MOGA, and the process leads back to (b).

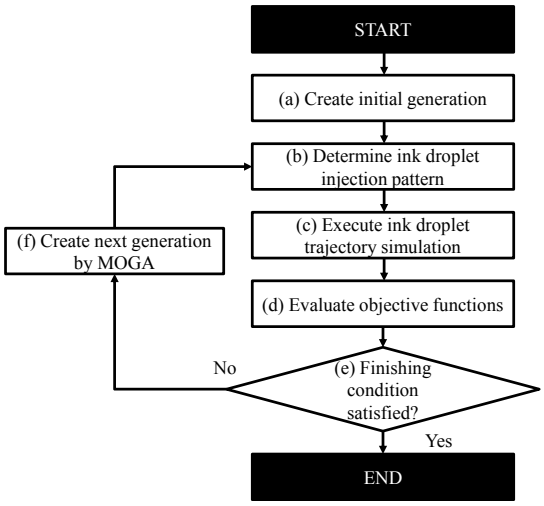


***Figure 8.*** *Printing quality optimization flow.*

**Table 2:** Optimization settings

| | |
|---|---|
| Algorithm | Multi-objective genetic algorithm |
| Generation | 4 |
| Population | 20 |
| Niching | Goldberg's sharing function [7] |
| Crossover method | BLX-$\alpha$ [4] |
| Mutation method | Non-uniform mutation [4] |

4. Printing control rules extraction

To extract the printing quality improvement rules, correlation analysis was performed. The analysis calculates correlations between the numbers of non-charged droplets at each injection timing position shown in Fig. 5 and the height error sum from the ideal heights of each horizontal line. The sample Pearson's correlation coefficients were calculated as follows:

$$r_{x_i x_j} = \frac{s_{x_i x_j}}{s_{x_i} s_{x_j}} = \frac{\sum_{k=1}^{n}(x_{ik} - \bar{x_i})(x_{jk} - \bar{x_j})}{\sqrt{(\sum_{k=1}^{n}(x_{ik} - \bar{x_i}))(\sum_{i=1}^{n}(x_{jk} - \bar{x_j}))}} \quad (8)$$

where $i, j$ are the value identifiers, $x_i, x_j$ are samples $(x_i = \{x_{ik}\}, x_j = \{x_{jk}\})$, $r_{x_i x_j}$ is the correlation coefficient, $s_{x_i x_j}$ is the sample covariance, $s_{x_i}$ *and* $s_{x_j}$ are the standard deviations of $x_i$ *and* $x_j$, respectively, $n$ is the number of samples, and $\bar{x_i}$ *and* $\bar{x_j}$ are the sample means of $x_i$ *and* $x_j$, respectively.

For all combinations of the number of non-charged droplets and the height error sums of each line, the correlation coefficients were calculated using Eq. (8). The timing positions of non-charged droplet injections strongly related to each height error sum were specified, and rules to reduce the height errors were extracted. Additionally, the extracted rules were applied to the characters "3" and "5," in which the ink droplet trajectory simulation was performed and the rules were validated.

## Result

Figure 9 shows a scatterplot of objective function values. The plot of "baseline pattern" expresses the values obtained from the simulation with the baseline injection pattern described in Fig. 6. Since two objective functions are both minimization targets, the orange rectangular region in Fig. 9 highlights values considered to be better than those of the baseline pattern in terms of objective function values. It was confirmed that the two errors as objective functions decreased during the MOGA generation.

The simulation results with the baseline pattern and the optimal injection pattern obtained by the MOGA shown in Fig. 9 were then compared. Figure 10 shows the hit positions on the printing target of each injection pattern. Horizontal dot lines correspond to the ideal heights of each line. The horizontal positions of dots 15 and 25 were too close in the simulation result of the baseline pattern. However, in the simulation result of the optimal pattern, the distance between those dots was wider. Additionally, the longitudinal positions of dots 32 54 in the simulation result of the baseline pattern were shifted from the ideal heights, whereas those in the simulation result of the optimal pattern hit on the ideal heights.

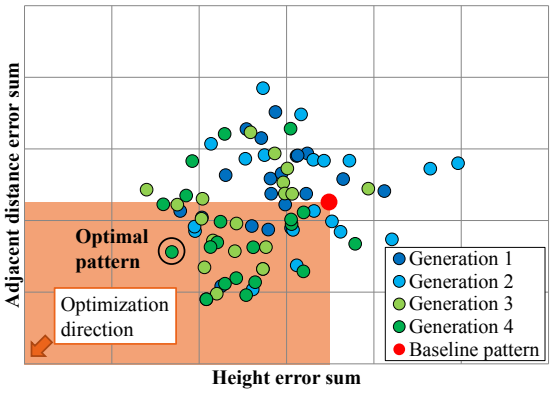


***Figure 9.*** *Scatterplot of two objective functions.*

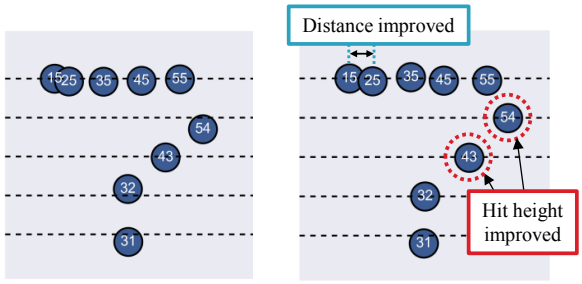


***Figure 10.*** *Simulation results of (a) the baseline injection pattern and (b) the optimal injection pattern of character "7". The optimal pattern could improve the horizontal distance and the hit height.*

Correlation analysis was then applied to the data obtained in the optimization process, and the rules for improving printing quality were extracted. These rules were applied to the characters "3" and "5" in a 5 × 5 dot matrix, and ink droplet trajectory simulations were performed. The simulation results are shown in Fig. 11. Figure 11 (a) and (c) are the simulation results of the baseline pattern of the characters "3" and "5" in which two non-charged droplets at the head of each column are injected as with the baseline pattern of character "7". Figure 11 (b) and (d) are the simulation results of the injection patterns of characters "3" and "5" to which the extracted rules were applied. Compared to the results of the baseline, although the hit positions of the lower dots were separate from the ideal heights, the highest dots hit close to the ideal height. Since the highest dots had a relatively large negative charge, the hit positions tended to be largely affected by Coulomb repulsion. Therefore, the adjustment of the hit position of the highest dots was more difficult than the lower dots. However, by using the extracted rules, the hit position of the highest dots could be adjusted automatically. As a result, the line distortions decreased and the printing qualities were improved. It was confirmed that the optimization procedure in this study is effective for improving the printing quality of CIJPs.

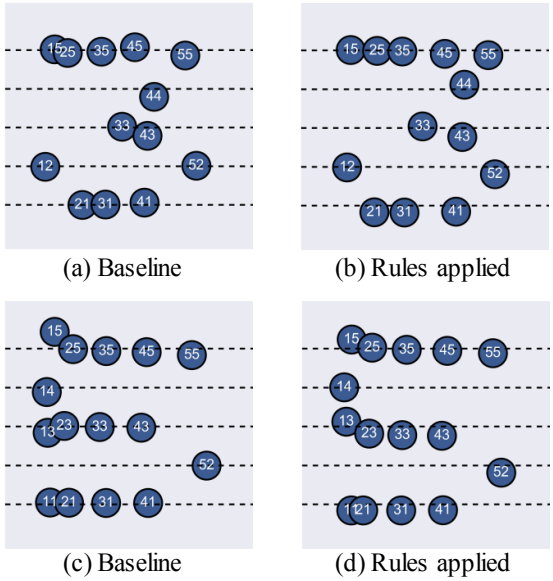


***Figure 11.*** *Simulation results of the baseline injection patterns and those in which the printing quality improvement rules were applied to of characters "3" and "5."*

## Conclusion

A printing quality optimization technique with a MOGA and ink droplet trajectory simulation was developed. The technique was applied to the character "7" in a 5 × 5 dot matrix.

1. The optimization technique could improve the printing quality of the character automatically, thus, it was confirmed that the developed technique worked appropriately.
2. The rules for improving printing quality from the optimization results of the character were extracted and applied to the characters "3" and "5." It was revealed that the extracted rules effectively improved the printing quality of the characters as well.
3. The developed technique can be used to determine the printing control method of CIJPs.

## References

[1] Ikegawa, M., Ishii, E., Harada, N., and Takagishi, T., "Development of Ink-Particle Flight Simulation for Continuous Inkjet Printers," Journal of Manufacturing Science and Engineering, Vol. 136, (2014).

[2] Beard, K. V., and Pruppacher, H. R., "A Determination of the Terminal Velocity and Drag of a Small Water Drops by Means of a Wind Tunnel," Journal of the Atmospheric Sciences, Vol. 26, pp. 1066–1072, (1969).

[3] Tsuji, Y., Morioka, Y., Terashima, K., Shiragami, T., and Ninomiya, H., "Fluiddynamic Interaction between Two Spheres," Transactions of the Japan Society of Mechanical Engineers, Series (B), Vol. 47, No. 423, pp. 2103–2110, (1981) [in Japanese].

[4] Deb, K., "Multi-Objective Optimization using Evolutionary Algorithms," John Wiley & Sons, (2001).

[5] Issa, R., "Solution of the Implicitly Discretized Fluid Flow Equations by Operator-Splitting," Journal of Computational physics, Vol. 62, Issue 1, pp. 40–65, (1986).

[6] McKay, M. D., Beckman, R. J., and Conover, W. J., "A Comparison of Three Methods for Selecting Values of Input Variables in the Analysis of Output from a Computer Code," Technometric, Vol. 21, No. 2, pp. 239–245, (1979).

[7] Goldberg, D. E., and Richardson, J., "Genetic algorithms with sharing for multimodal function optimization," Proceedings of The Second International Conference on Genetic algorithms and their application, pp. 41–49, (1987).

## Author Biography

*Koma Sato obtained his master's degree in information science at Tohoku University in Japan in 2007. His thesis was on the total body shape optimization of a supersonic business jet in the group of Prof. Obayashi (Institute of Fluid Science, Tohoku University). He joined Hitachi Ltd. in 2008 and has been engaged in studies about the design of industrial products using computational fluid dynamics, optimization methods, and data science techniques.*